Limbic and cerebellar effects in Alzheimer-Perusini's disease: A physics-inspired approach

Maria Mannone [a,b,c],*, Norbert Marwan [b,d,e], Peppino Fazio [c,f], Patrizia Ribino [a]

[a] ICAR, National Research Council (CNR), Palermo, Italy
[b] Institute of Physics and Astronomy, University of Potsdam, Potsdam, 14476, Germany
[c] DSMN, Ca' Foscari University of Venice, 30170, Venezia Mestre, Italy
[d] Potsdam Institute for Climate Impact Research (PIK), Member of the Leibniz Association, 14473, Potsdam, Germany
[e] Institute of Geosciences Potsdam, University of Potsdam, 14476, Potsdam, Germany
[f] Department of Telecommunications, VSB - Technical University of Ostrava, 70800, Czechia

ARTICLE INFO

ABSTRACT

Alzheimer-Perusini's disease (AD) is a severe neurodegenerative pathology mostly characterized by memory loss, with aging as a significant risk factor. While normal aging involves non-pathological changes in the brain, pathological aging involves the formation of neuronal plaques, leading to neuronal death and the macroscopic shrinkage of major brain regions. Prodromic dopaminergic alterations also affect the limbic system. We adopt a physics-inspired mathematical operator, the *Krankheit-Operator*, denoted as K, to model brain network impairment caused by a neurological disorder. By acting on a pathological brain, K plays a role in modulating disease progression.

The evaluation of the K-operator is conducted across different stages, from cognitive normal (CN) to Mild Cognitive Impairment (MCI) and AD. Furthermore, by adopting a machine learning-based approach, we also explore the potential use of the K-operator as a diagnostic tool for predicting AD progression by starting from rs-fMRI at the initial visit. Our findings are consistent with the literature on the effects of AD on the limbic system, subcortical areas, cerebellum, and temporal lobe.

His own face in the mirror, his own hands, surprised him every time he saw them. [...] He was the solitary and lucid spectator of a multiform, instantaneous and almost intolerably precise world. [...] It was very difficult for him to sleep. To sleep is to turn one's mind from the world; Funes, lying on his back on his cot in the shadows, could imagine every crevice and every molding in the sharply defined houses surrounding him. [1]

1. Introduction

In medio stat virtus: the virtue resides in the middle, in the equilibrium, as Ancient Romans used to say. In a different culture, as the Chinese one, there is a similar concept, with the character 中 indicating "middle"—and the country itself is named after it. Cultures are the product of a collection of brains over time and each human, to function properly, needs a balance—balance of electrical impulses, neurotransmitters, blood, glucose, and water. The identity of cultures requires memory, as well as the identity of the individual. In Chinese, *brain* is literally a *container of memory* and intelligence, 脑.[1] But memory itself needs a balance. A brain that cannot forget anything is suffering, as Funes in Borges' tale [2]. This is an example of what has been recently identified as *hyperthymesia* [3,4]. Conversely, a brain that is too forgetting, lets little by little, disintegrate the individual's identity.

Loss of memory is one of the symptoms of Alzheimer's disease (AD), which we will be calling here Alzheimer-Perusini's disease for historical reasons [5]. AD is a serious neurodegenerative pathology that includes aging as a risk factor. While normal aging implies a non-pathological transformation of the brain, as in the calcarine cortex [6], pathological aging may include the formation of plaques inside neurons, causing their death, and the macroscopic effect of shrinking of main brain regions. Brain damage provoked by AD has effects on short-term
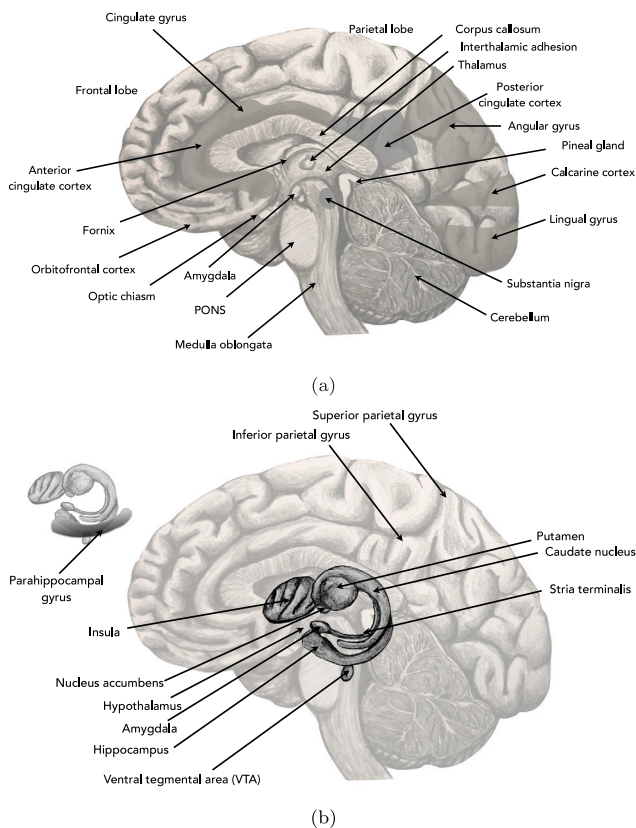

Fig. 1. Some salient areas of the brain (a) and the detail of parts of the limbic system and insula (b), with some dopaminergic centers, such as nucleus accumbens, ventral tegmental area, and stria terminalis. Drawing by M. Mannone.

memory, mostly involving the prefrontal lobe, and long-term memory, concerning the posterior parietal cortex [7].

Memory consolidation involves the hippocampus, one of the areas targeted by AD, as well as the parahippocampal gyrus, fusiform, and entorhinal cortex, which have a crucial role in memory [8]. That the hippocampus is crucial for memory was witnessed by the story of patient H. M. [9].[2] AD also affects, among many brain areas, the core parts of the limbic system, that is, the hippocampus and amygdala [10] (see Figs. 1(a) and 1(b), and Rubin and Safdieh [11]).

In this study, we detect brain areas involved in AD progression using a method inspired by physics. In theoretical physics, the changes in a system, described by a matrix, can be induced by the action of an operator, also described by a matrix. The human brain can be considered as a complex network: a physical network if we focus on connected neurons or a functional network considering connected regions. Let us choose the second perspective, treating the brain mathematically as a matrix, whose elements are the weights of links between brain regions. In this way, it is possible to formalize the action of some diseases related to pathological changes in the connectivity of neurons or brain regions as an operator acting on the functional network: the so-called K-operator, where K stands for *Krankheit*, German for *disease* [12]. We identify the brain matrix as the connectivity matrix, with information about the strength of the connections between brain areas.

Encouraged by the promising results obtained by the first application of the K-operator to real data, in the framework of Parkinson's

---

[2] As part of a surgery to stop epileptic seizures, Henri Gustav Molaison got removed several brain areas, including part of the hippocampus, hippocampal gyrus, entorhinal, amygdala. As a result, he developed severe anterograde amnesia.

Disease [13], and wanting to find a "signature K" characterizing different diseases, as theoretically mentioned in Mannone et al. [14], here we apply K to the Alzheimer-Perusini's disease. Mainly, focusing on selected patients from the Alzheimer's Disease Neuroimaging Initiative (ADNI) and using tools from matrix computation, we determined experimental instances of K and identified the more targeted areas of the brain. Then, we compared our results with the literature on the field, and we also explored the potential use of the K-operator as a diagnostic tool for predicting AD progression starting from rs-fMRI at the initial visit.

This study is the extension of a first analysis [15], with the inclusion of all brain areas, the Automatic Anatomic Labeling version 3 (AAL3) atlas [16] for more details on the temporal lobes and limbic system, and the use of a multi-layer perceptron for the prediction of disease progression. In our comments, we will focus more on the role of the temporal lobe, hippocampus, parahippocampal gyrus, amygdala, cerebellum, vermis, nucleus accumbens, and part of the dopaminergic pathway. In fact, the balance of dopamine is essential for the correct functioning of memory [17].

Our work is contextualized within the flourishing research area of brain-network analysis, bridging physics-based modeling with medical applications [18], from neuronal interactions to neural agglomerates [19] and masses [20], to whole-brain analysis. Our contribution is two-fold: on the one hand, we aim to find disease-specific information, confirming the literature results and developing a new predictive approach; on the other hand, we want to develop, piece after piece, a general theory of the connectome-based neurological disease with the tools of theoretical physics. Concerning this last aspect, our research tries to answer the quest for a more general (and theoretical) approach to neurological disease, aiming to foster new therapies [21]. A theoretical framework can help collect and frame the vast knowledge coming from experimental studies on brain networks, such as the studies on epilepsy [22], AD [23], and schizophrenia [24].

The rest of the paper is organized as follows. Section 2 introduces the formalization of the K-operators and all materials and methods used in the present study. Section 3 presents an experimental evaluation of the proposed approach on a cohort of subjects selected from the ADNI dataset. Section 4 investigates the potential application of the K-operator as a diagnostic tool in predicting the progression of Alzheimer-Perusini's disease. Finally, Discussions and conclusions are respectively presented in Sections 5 and 6.

2. Materials and methods

2.1. K-Operator formalization

The functional connectome denotes a detailed representation of neural connections within the brain. By delineating the brain into distinct regions of interest (ROIs), the connectome can be represented as a connectivity matrix, which quantifies and characterizes the interactions among these regions. Statistical measures, including correlation coefficients, are employed to evaluate the degree of co-activation between pairs of ROIs. These measures are computed using a designated brain atlas, resulting in weighted connectivity matrices that reflect the strength of connections between the corresponding ROIs. Each element within a connectivity matrix indicates the correlation observed between a pair of ROIs.

Hence, according to our notation [12], the brain network is represented as a block matrix denoted by $\mathcal{G}$. In this matrix, each diagonal block corresponds to the connections within brain lobes, while the off-diagonal blocks represent the inter-lobe connections. The *Krankheit-Operator*, in short K-operator, acts upon the healthy brain $\mathcal{G}$ to generate a resulting state of the brain denoted as $\mathcal{G}^k$, characterized by disease manifestations:

$$K\mathcal{G} = \mathcal{G}^k \tag{1}$$

where the specific form of K depends upon the disease under study. Thus, considering as the starting point a brain already affected by the disease, K can model its progression as

$$K(t)\mathcal{G}^k(t) = \mathcal{G}^k(t+1), \tag{2}$$

where $\mathcal{G}^k(t)$ is the diseased-brain matrix at time t, and $\mathcal{G}^k(t+1)$ at the following time-point. Thus, using $\mathcal{G}^k(t)$ and $\mathcal{G}^k(t+1)$ as the connectivity matrices of the brain network of the same patient at two different time points, and provided that $\mathcal{G}^k(t)$ is invertible, we can obtain the K-operator as

$$K(t) = \mathcal{G}^k(t+1)\left[\mathcal{G}^k(t)\right]^{-1} \tag{3}$$

Two different strategies are considered here for computing the elements of K: the classic row-by-column product and a hybrid one computing the elements of K using the element-wise product. The classic one is more precise and formally justified, while the second one allows for better readability thanks to its symmetry and correspondence with the actual ROI-ROI pairs. We indicate the hybrid product (element-wise) with $*$, and the classic product with @, the corresponding symbols in Python. The i, j-th matrix elements of K are obtained as in Eq. (4) and (5), respectively:

$$K_{ij}^* = \left(\mathcal{G}_{n^t+1}^k\right)_{ij}\left(\left[\mathcal{G}_t^k\right]^{-1}\right)_{ij} \tag{4}$$

$$K_{ij}^@ = \sum_{l=i}\left(\mathcal{G}_{t+1}^k\right)_{il}\left(\left[\mathcal{G}_t^k\right]^{-1}\right)_{lj}, \tag{5}$$

where K_{ij}^* and $K_{ij}^@$ are the ij-th elements of K computed via two different products, respectively: element-wise in Eq. (4), and with the usual matrix product in Eq. (5).

The two formulas are different, but thanks to the similar sparsity of information, patterns and clusters correspond. Empirically, the element-wise technique allows us to find the brain regions more affected by the disease; the classic product detects exactly the action of K on them. The correspondence between main blocks found with both products is shown in the Appendix (Fig. 12).

2.2. ADNI dataset

The present study relies on data gathered from ADNI,[3] specifically focusing on the data derived from the ADNI 2 study. Such a study is a longitudinal investigation designed to identify and monitor clinical, imaging, genetic, and biochemical biomarkers for early AD detection.

ADNI categorizes different AD stages for participants as healthy normal control CN, Subjective Memory Complaints (SMCs), Mild Cognitive Impairment (MCI), and Alzheimer-Perusini's Disease (AD) classes. In particular, ADNI 2 distinguished Mild Cognitive Impairment (MCI) into Early MCI (EMCI) and Late MCI (LMCI). The progression from the EMCI stage to the LMCI is not reversible, which means that the patient's cognitive condition gets worse significantly.

Among the several features provided by ADNI 2, we focus on neuroimaging features, i.e., resting-state functional magnetic resonance imaging (rs-fMRI). We mainly considered rs-fMRI connectivity analysis for identifying neurodegenerative diseases characterized by disruptions in brain network connectivity before the onset of observable brain atrophy. In ADNI, the rs-fMRI images were collected at baseline, three months, six months, 12 months from baseline, and annually afterward.

This study selected seven subjects from four classes from ADNI: CNs, EMCI, LMCI, and AD patients. According to ADNI inclusion criteria, the Mini-Mental State Exam (MMSE) score for CN, EMCI, and LMCI is between 24 and 30. While the MMSE score for AD is between 20 and 26.

Dementia status was also assessed using the Clinical Dementia Rating (CDR) Score. The CDR Staging Instrument [25] is commonly utilized to characterize cognitive and functional performance across six domains relevant to AD, including Memory, Orientation, Judgment and Problem-Solving, Community&Affairs, Home&Hobbies, and Personal Care. The CDR assessment produces a CDR global score (CDR-GS) and a CDR sum of Box (CDR-SOB). CDR-GS is calculated via an algorithm with defined scoring rules [25] based on the scores of the aforementioned domains. On the contrary, the CDR-SOB is the sum of each domain score. As opposed to the CDR-GS, which is a 5-point ordinal scale ranging from 0 to 3 (no cognitive impairment = 0, MCI = 0.5, mild = 1, moderate = 2, severe = 3), the CDR-SB is a continuous measure of dementia severity ranging from 0 (no cognitive impairment) to 18 (severe cognitive impairment).

2.3. Medical images and methodological steps

The rs-fMRI [26] is a method that involves the examination of low-frequency fluctuations in the blood-oxygen-level dependent (BOLD) signal when an individual is not engaged in any tasks or exposed to external stimuli (i.e, in a state of rest). The BOLD signal exhibits fluctuations with a high degree of temporal coherence across spatially segregated regions that are functionally linked, forming the foundation of distinct sensory, motor, and cognitive networks. Hence, BOLD functional connectivity (BOLD-FC) derived from rs-fMRI is considered a reliable indicator of neuronal connectivity. In a range of neurological disorders, disruptions in metabolism, blood flow, and dynamic cardiovascular function likely give rise to variations in BOLD-FC that differ from changes in neuronal activity. Scanners used to acquire rs-fMRI images usually store data in the DICOM format. The Digital Imaging and Communications in Medicine (DICOM) [27] standard specifies a non-proprietary data interchange protocol, digital image format, and file structure for biomedical images and image-related information. Since DICOM is a vast and complicated standard, the NIfTI file format is frequently employed in medical imaging research due to its relative simplicity as a data format and its minimal inclusion of identifiable patient data and metadata fields.

Therefore, to implement the proposed K-operator for modeling Alzheimer-Perusini's disease, we perform the following three steps:

(i) *Data preprocessing*: we convert the rs-fMRI data from DICOM to NIfTI format by adopting the *dicom2nifti* Python library.[4]
(ii) *Connectome Extractions*: brain network and connectivity are obtained by processing the NIfTI files with the *nilearn* Python library.[5] In particular, we extract time series for each region of interest (ROI) in which the brain can be divided according to a specific choice of atlas and then compute the connectivity matrices.
(iii) *K-operator determination*: we compute the shapes of the K-operator experimentally in matrix form, and we visualize the connectivity matrices for the brain networks, with the brain regions grouped into ROIs.

2.4. Medical atlases

Medical images are composed of different voxels. By grouping the voxels, information can be gained on specific brain areas. The choice, size, and distribution of voxel grouping depend upon the specific medical atlas. In our previous study [15], the adopted atlases were MSDL and a selection of areas from Oxford [28,29]. Here, we use the AAL3 atlas [30], a development of AAL and AAL2 [16,31], with a more detailed segmentation of the thalamus, and the inclusion of further areas, such as the ventral tegmental area (VTA), the nucleus accumbens, and the substantia nigra (pars compacta is visible in our

---

[3] Accessible at www.loni.ucla.edu/ADNI.

[4] Available at https://pypi.org/project/dicom2nifti/
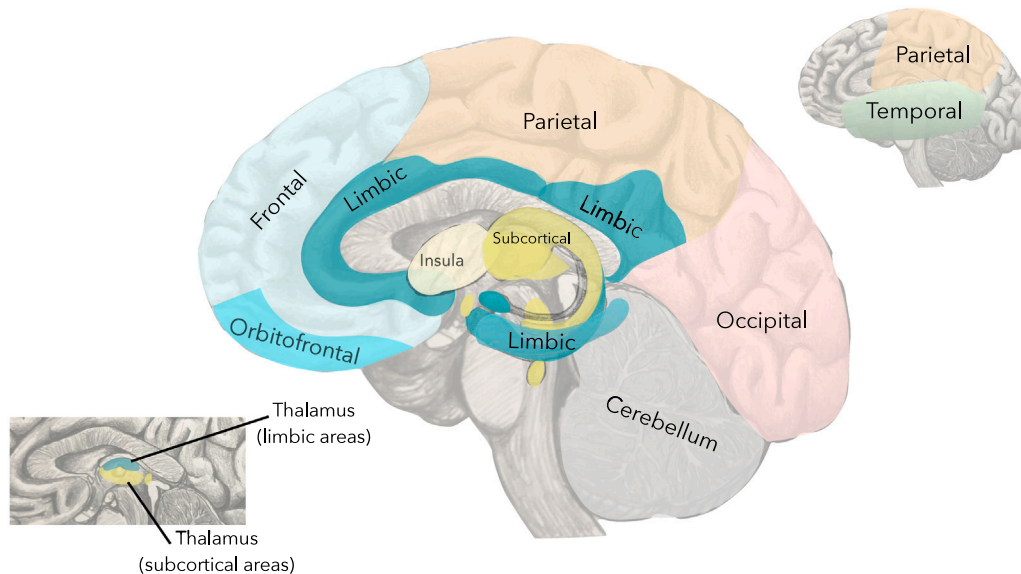[5] Available at https://nilearn.github.io/stable/index.html

Fig. 2. Distribution of the main areas of the brain [14].

data, not the pars reticulata), that is, some of the key areas of the dopaminergic circuit.

Relationships between AD and VTA are described by [32]. Damage to the nucleus accumbens is one of the prodromic signs of AD, appearing before the alteration to the hippocampus [33]. Locus ceruleus (LC) also has a key role in AD [34]. For instance, one of the AD signs is the loss of neurons in the LC and in the thalamic relay nuclei, significantly higher than in healthy patients [34]. However, the data available to us misses a voxel readability in correspondence with the LC, and thus, we do not include this in our analyses.

Table A.3 in Appendix lists the ROIs from the AAL3 atlas used in our analyses and their approximated distribution according to the brain lobes (all ROIs in Table A.3 are colored according to the brain lobes in Fig. 2). There is a limbic and a subcortical part of the thalamus. The limbic part, called *limbic thalamus*, includes anterior nuclei, midline nuclei, mediodorsal-nucleus medial division (MDm), and central medial nucleus (CM) inside the intralaminar complex [35]. There is a single ROI for the intralaminar nuclei (IL) of the thalamus that contains Central medial (CeM), Central lateral (CL), Paracentral (Pc), Centromedian (CM), and Parafascicular (Pf) nuclei [16]. The Centromedian is a limbic system part, but for the sake of simplicity, the overall IL is marked as "subcortical" (mustard color) in Table A.3.

2.5. Multi layer perceptron for K-operator prediction

Given the connectivity matrix of a new patient at the baseline, the prediction of K can potentially provide significant prognostic insights into the progression of the patient's disease. Through these techniques, we can perform an "internal validation" of the K-operator, not only relying on medical literature but also on the similarity between predicted numerical entries of the operator and the actual evolution of the patient, comparing the predicted with the measured evolution of the disease. In this paper, we adopt a machine learning-based approach to predict the shape of the K-operator differently from our previous work, in which a simple linear regression was used. In particular, here we adopt a Multilayer Perceptron (MLP), a type of artificial neural network characterized by a fully connected architecture comprised of neurons with non-linear activation functions, allowing the network to learn complex patterns in data. The MLP developed for the K-operator prediction is structured in three layers with 64 neurons that employ the

rectifier activation function (ReLU). The Adaptive Moment Estimation (Adam) optimizer is used to minimize the loss function during the neural network training. Summarizing, the hyperparameters considered to tune our system are: 64 as the number of neurons, 50 as the epochs, 3 hidden layers, ReLU as the activation function, Adam as the optimizer, batch size as 32 by default.

3. K-Operator experimental evaluation

3.1. Patients selection

For the experimental evaluation of K-operator, we chose patients with rs-fMRI from ADNI, which contains all the necessary elements for our computation. Then, for the purpose of our study, we select seven patients from the ADNI dataset subgroups with the following characteristics:

- patient A (ID: 019_S_5019) is a 63-year-old AD female with a middle-low education level (i.e., 12 years), an MMSE score of 21, showing problems in each CDR domain with a CDR-SB = 6 and CDR = 1;
- patient B (ID: 002_S_5018) is a 73-year-old AD male with a middle-high education level (i.e., 17 years), an MMSE score of 23, showing minor problems than patient A in the domain of Community&Affair and Home&Hobby with a resulting CDR-SB = 5 and CDR = 1;
- patient C (ID: 006_S_4153) is a 79-year-old AD male with a high education level (i.e., 20 years), an MMSE of 22, with minor problems than patients A and B in all domains with CDR-SB = 3 and CDR = 0.5;
- patient D (ID: 018_S_4399) is a 78-year-old CN female with a middle-high education level (i.e., 16 years), an MMSE of 28, without any problems in each domain with a resulting CDR-SB = 0 and CDR = 0;
- patient E (ID: 012_S_4012) is a 71-year-old EMCI female with a middle-high education level (i.e., 16 years), an MMSE of 28, initial problems in Memory, Orientation, and Judgement, CDR-SB = 1.5 and CDR = 0.5;

Table 1

Patients' characteristics. *Educ.* stands for the years of education, and *Sect.* indicates the sections of the article where they are considered. *Patient C was used as test of the prediction.

Patient	ID	Sex	Age	Educ.	Group	MMSE	CDR-SB	CDR	Sect.
A	19_S_5019	F	63	12	AD	21	6	1	3.2
B	02_S_5018	M	73	17	AD	23	5	1	3.2
C*	006_S_415	M	79	20	AD	22	3	0.5	4
D	018_S_4399	F	78	16	CN	28	0	0	3.3
E	012_S_4012	F	71	16	EMCI	28	1.5	0.5	3.3
F	031_S_4203	F	77	17	LMCI	26	4	0.5	3.3
G	018_S_4696	F	73	16	AD	16	9	1	3.3

- patient F (ID: 031_S_4203) is a 77-year-old LMCI female with a middle-high education level (i.e., 17 years), an MMSE of 26, with higher problems in Memory, Orientation, and Judgement than Patient E and initial problem in Home&Hobby domain with a CDR-SB = 4 and CDR = 0.5;
- patient G (ID: 018_S_4696) is a 73-year-old AD female with a middle-high education level (i.e., 16 years), an MMSE of 16, showing higher problems in Memory, Orientation, and Judgment than patient F, and higher problem in Home&Hobby and personal care with a resulting CDR-SB = 9 and CDR = 1.

The last four patients were selected to evaluate the evolution of the K-operator in AD progression. Since we do not find patients with associate rs_fMRI images that show all the stages of AD progression, we select these patients according to statistical findings we reported previously [15]. We summarize the characteristics of considered patients in Table 1.

3.2. Evaluation of K-operators for AD patients

We compute K for most of our analysis by using Eq. (4), and for some comparisons, with Eq. (5), where indicated. Here, we focus on evaluating K-operators for patients A and B. The K-operator was computed on their rs-fMRI using the AAL3 Atlas at two different time points: the baseline and the first follow-up visit.

To highlight the most affected regions, we consider the highest values of the K-operator for patients A and B obtained by adopting an empirical threshold of 0.3 and 0.1 respectively (Figs. 3(a) and 3(b)). It is worth noting that we use thresholds to visually emphasize the higher values of the operator and focus on the corresponding brain areas.

Regarding patient A, the most deactivated areas are the frontal inferior orbitofrontal cortex (OCF), medial-anterior and lateral orbital gyrus, occipital superior, occipital inferior, postcentral, and parietal, accumbens and ventral tegmental area. Connectivity is increased between the fusiform and frontal superior, the motor area and the anterior cingulate cortex, and other disruptions involve the frontal medial and orbital and the thalamus pulvinar anterior and medial.

For Patient B, clusters of K action are mostly in the precentral and frontal lobe, between cerebellum crus right and left and lingual gyrus, and between nucleus accumbens and putamen, between amygdala and cuneus, lingual, and occipital, between nucleus accumbens and anterior cingulate cortex.

Both patient A and patient B present an alteration of connectivity between the amygdala and parahippocampal gyrus, frontal area, and between the ventral tegmental area and the anterior cingulate cortex. The last one has a decisive role in connecting the limbic system, more related to feeling, emotion, arousal, and motivation, with the prefrontal cortex, related to cognition and conscious decision-making [36]. Inside the limbic system, let us focus on the ventral tegmental area (VTA), which is part of the dopaminergic system. Dysfunctions of both VTA and anterior cingulate cortex are connected to neuropsychiatric disorders occurring in AD [32,36]. Given the importance of parahippocampal gyrus for memory, the aforementioned areas are key to AD,
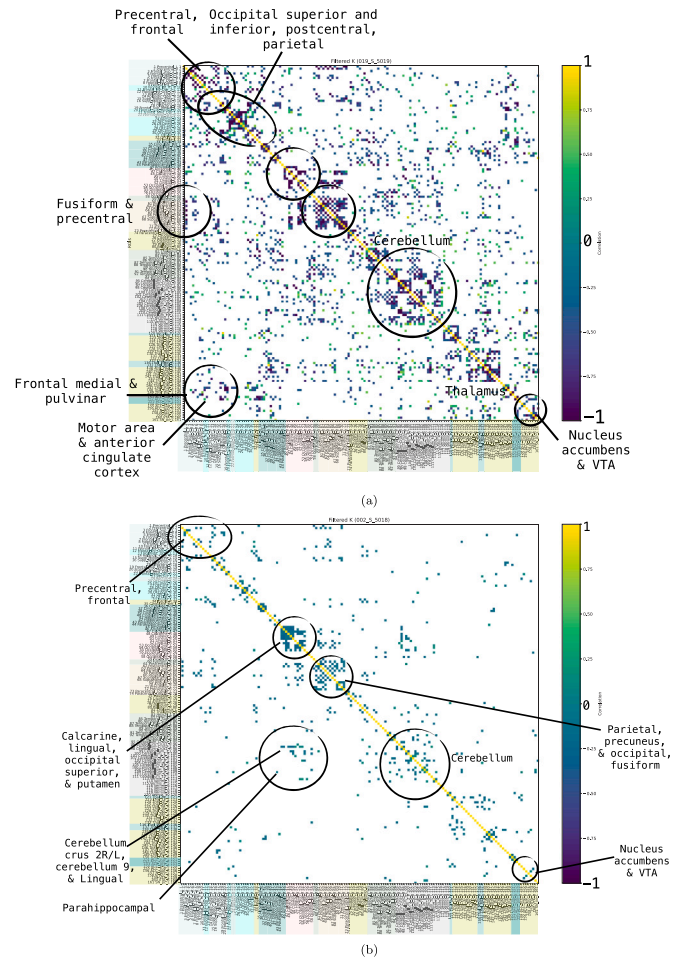

Fig. 3. K-operator for patient A and patient B (colors as in Fig. 2).

from memory to cognition to neuropsychiatric disorder. Alteration of VTA is also relevant for Parkinson's disease [37].

In fact, dopaminergic drugs used for PD also have a positive effect on AD patients to slow down the disease progression [32]. Another common aspect between A and B is the damage to connectivity between some cerebellar areas and the temporal lobe. The diminution of long-range connection in the brain is another sign of AD [38].

In summary, we can relate the effects found with the K-operator to other observations on the same patients concerning memory, judgment (cognition), and orientation (linked to the cerebellum).

Some differences concern diminished connectivity between the motor area, olfactory, and anterior cingulate cortex for patient A, which is rather a small increase for Patient B, similarly to the alteration of the connectivity between the caudate, putamen, and accumbens.

To provide a more detailed view of the K-operator's action and visual insights into the symmetry of brain connectivity, we visualize the connectomes showing the links most affected by the disease at baseline and follow-up. We mainly show the links corresponding to the higher values of K above an empirically chosen threshold, see Figg. 4 and 5 for patients A and B, respectively.

We will list some key features compared to the study by [38]. In that work, the emphasis is on vertex connectivity; here, we mostly focus on links.

The comparison between the baseline and the follow-up connectome for Patient A (Fig. 4) shows a disease progression. Mainly, we notice an alteration of connectivity concerning the vermis and the cerebellar area. The decrease in the the occipital lobe confirms the findings
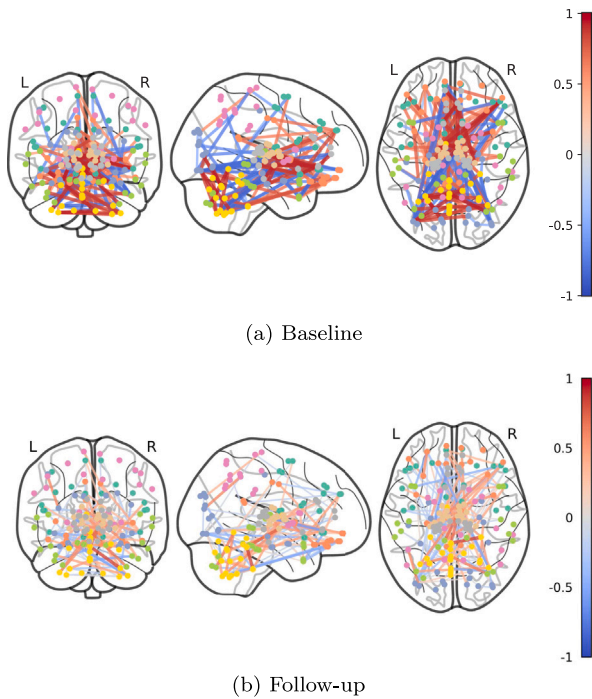
(a) Baseline

(b) Follow-up

Fig. 4. Baseline and follow-up connectome of patient A with only the links corresponding to all the areas more affected by K (threshold 0.2).
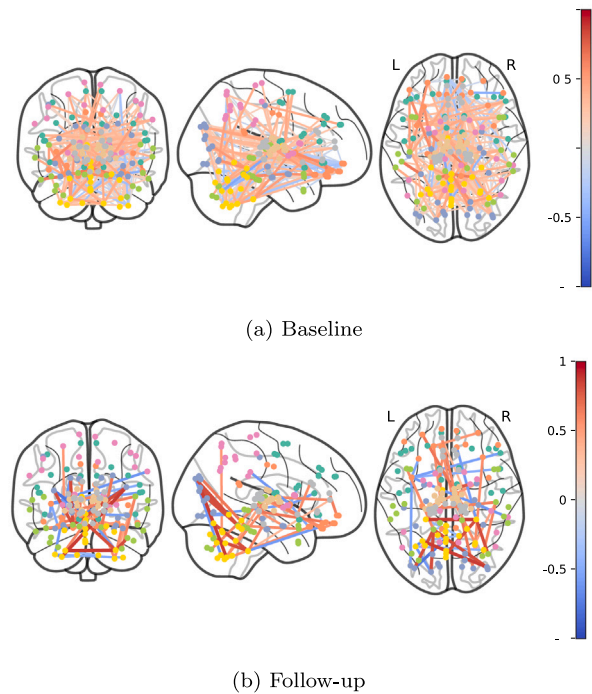

(a) Baseline

(b) Follow-up

Fig. 5. Baseline and follow-up connectome of Patient B with only the links corresponding to all the areas more affected by K (threshold 0.05 and 0.09, respectively).

of [38] and our previous findings in [15]. We also notice a decrease of connectivity in the temporal area and in the frontal lobe.

The connectome for Patient B, at the baseline (Fig. 5(a)) and at the first follow-up (Fig. 5(b)), confirm the findings by [38] concerning the increase of cerebellar (and in particular of vermis) and frontal

connectivity, and the diminution of occipital connectivity. Overall, we confirm the general trend of strength diminution of long-range links and the increase of strength in local links. This implies a change in the topology of the brain network.

3.3. Evaluation of K-operator in AD progression

Alzheimer-Perusini's disease is characterized by gradual and irreversible degeneration of the brain. It encompasses a lengthy preclinical period spanning up to two decades, followed by an average clinical course lasting 8 to 10 years. AD development is characterized by alterations in the brain that serve as biomarkers of the disease. This section's objective is to examine the functional brain network in individuals with Alzheimer-Perusini's disease and mild cognitive impairment, categorized as Early (EMCI) and Late Mild Cognitive Impairment (LMCI), as well as healthy individuals. This investigation seeks to evaluate through the K-operator the association between healthy brain network functional connectivity and the patterns of brain connectivity changes observed in patients across the AD spectrum. In this Section, we consider the brain connectome of four different female subjects (patients D to G) within the same range of age, from a healthy state to AD, aiming to investigate the variations provoked by the disease across time.

Fig. 6 shows the forms of the K-operator during the AD stages by adopting an empirical threshold of 0.05, respectively, obtained as:

$$K_1 : \text{CN} \rightarrow \text{EMCI}, K_2 : \text{EMCI} \rightarrow \text{LMCI}, K_3 : \text{LMCI} \rightarrow \text{AD},$$
$$K_4 : \text{CN} \rightarrow \text{AD}. \tag{6}$$

Observing the transition from CN to EMCI (Fig. 6(a)), we find the main impact of the disease on the prefrontal area, between the amygdala and occipital lobe, and between the ventral tegmental area and nucleus accumbens. This last information is particularly relevant, as alteration concerning VTA and nucleus accumbens are among the prodromic symptoms of AD [32,39].

The amygdala is related to the processing of emotions, and the alteration of its workings contributes to psychiatric illness. It is relatively less investigated in the AD framework; nevertheless, the amygdala also plays a role in its progression. According to some studies, alterations of the amygdala do also play a role in memory impairment, for instance, concerning hyperthymesia [3], which is somehow the opposite of AD. One of the reasons for the limited focus on the amygdala for AD studies is the difficulty of isolating it with respect to other brain areas. In addition, the greatest symptom of AD is memory loss, and thus, researchers are more focused on the hippocampus, parahippocampal gyrus, and entorhinal cortex. The pathological workings of the amygdala have been investigated more in psychiatric illnesses such as schizophrenia. According to [40], the effects of AD on the amygdala are now fully recognized. They can be helpful for early AD diagnosis, as they can appear even before the typical effects of memory decay. AD-induced damage on the calcarine cortex (within the occipital lobe) is limited; aging provokes greater damage [6]. Thus, focusing on the calcarine cortex may provide insights into the joint or different actions of aging and neurodegeneration, that is, healthy or non-healthy neuronal time-related alteration.

The EMCI → LMCI progression is not reversible, meaning that the patient's cognitive condition gets significantly worse. In such a transition (Fig. 6(b)), as in the previous one, we can observe effects between VTA and nucleus accumbens. The K-operator also shows relevant effects on cerebellum crus 1/2, cerebellum 4/5 R, 6R, and 6L. Indeed, the cerebellum primarily controls muscle, including balance and movement, and plays a role in cognitive functions, such as language and memory. The alteration in the cerebellum is consistent with the symptoms of decline in motor, cognition, and emotional activities since the cerebellum regulates these functions [41,42].
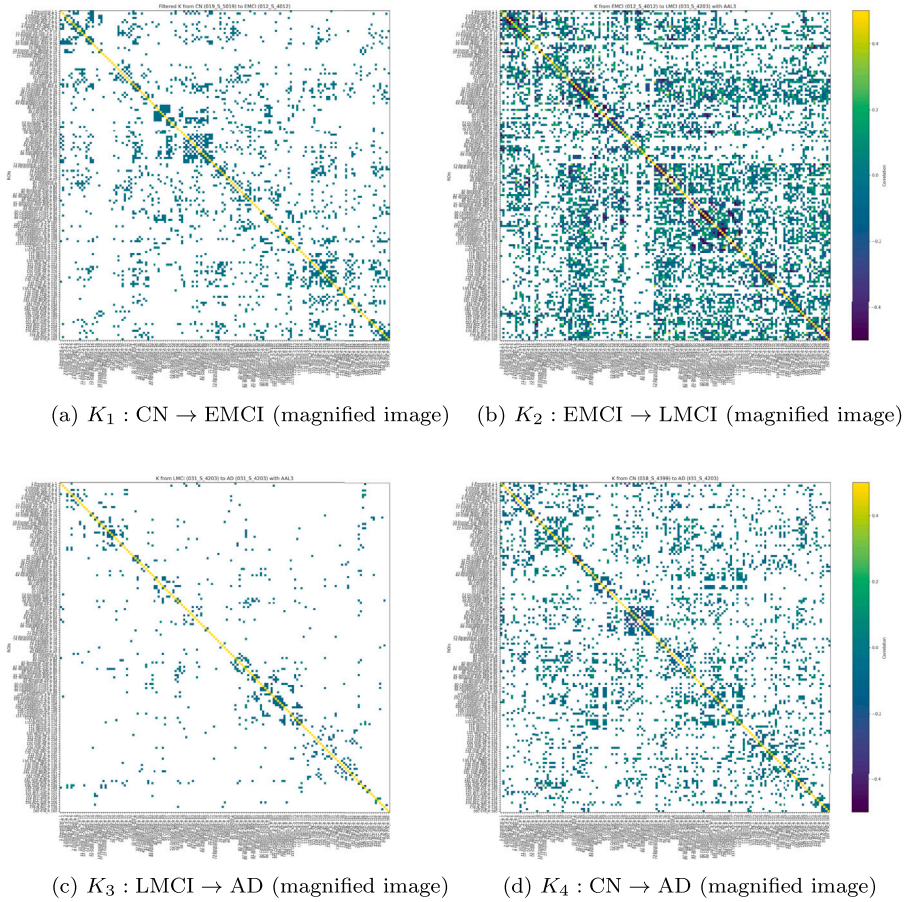
(a) $K_1 : CN \rightarrow EMCI$ (magnified image)

(b) $K_2 : EMCI \rightarrow LMCI$ (magnified image)

(c) $K_3 : LMCI \rightarrow AD$ (magnified image)

(d) $K_4 : CN \rightarrow AD$ (magnified image)
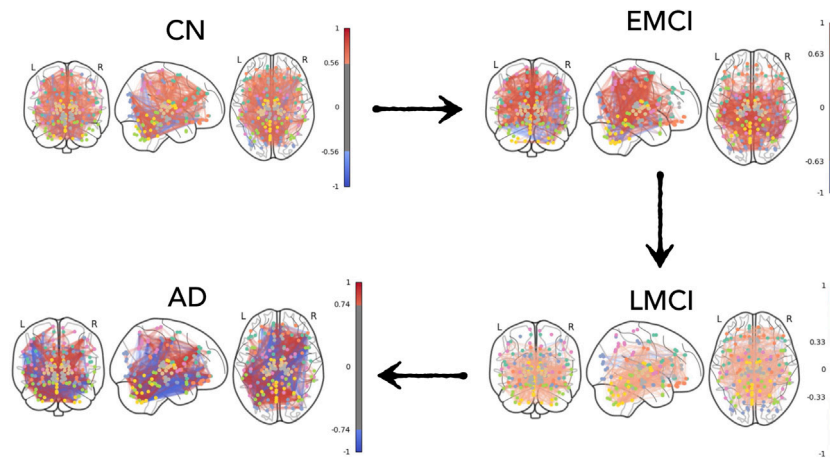
Fig. 6. K-operator for AD Progression.

Fig. 7. Connectomes comparison of female patients in the same age range, at different stages: from healthy control (CN) to early mild cognitive impairment (EMCI), to late MCI (LMCI), to Alzheimer-Perusini's disease (AD). Click here to magnify figure.

The LMCI → AD transition is less dramatic, probably because of the already-existing damage and the non-linear disease progression, as shown in [38]. Particularly, an effect of the disease on the orbitofrontal gyrus and cerebellum from 6R to 9R is visible (Fig. 6(c)). Comparing our results with [43], we confirm the connectivity alterations found from lobule VI (V in [38]) to IX of the cerebellum, orbitofrontal gyrus, and insula. The connectivity variation in the occipital pole was also visible in the previous stages.

Directly comparing the transition from CN → AD, the filtered K (Fig. 6(d)) presents peaks mostly in the amygdala, occipital inferior left,

cerebellum 8 R, and vermis 9, between VTA and nucleus accumbens, and the latter and anterior cingulate cortex, pulvinar with the cingulate cortex, lingual gyrus and insula, hippocampus and cingulate posterior, precuneus, fusiform with occipital. Consequently, AD individuals exhibit a similar pattern of brain injury diffusion when compared to healthy controls.

Moving to the glass-brain representation of connectomes, focusing only on the 20% stronger links in absolute value, we consider the temporal evolution of the progression from CN to AD of patients D to G (see Fig. 7). Cerebellar effects are among the first visible changes
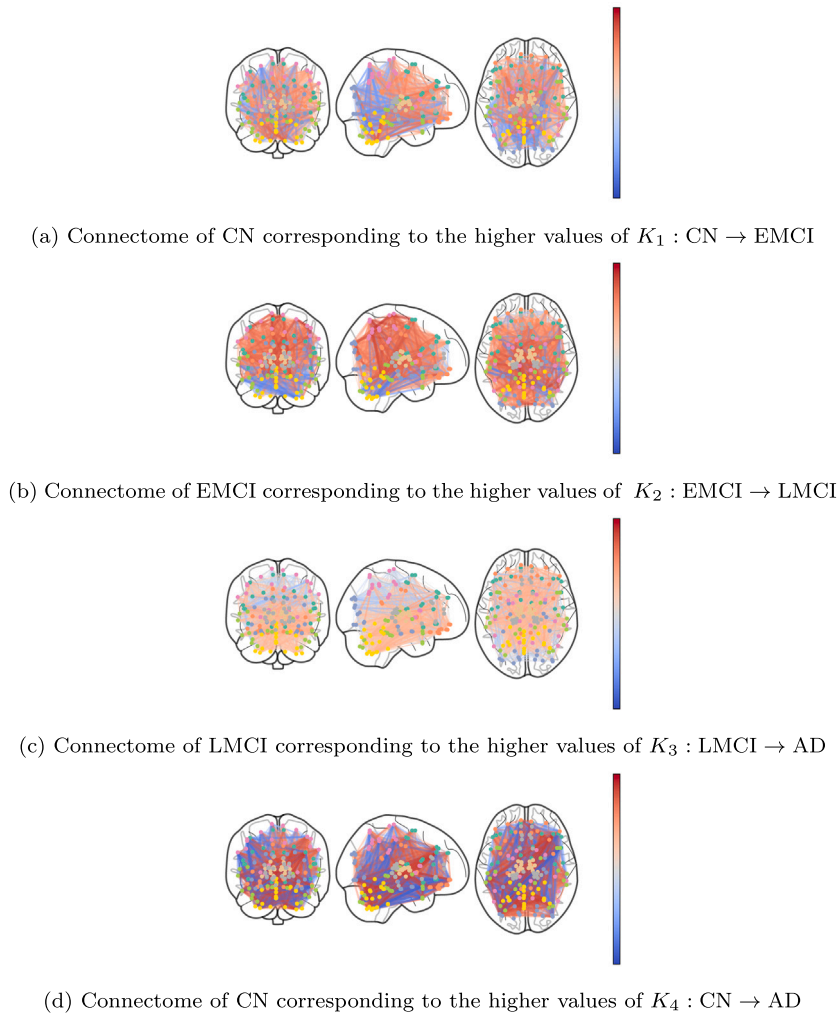
(a) Connectome of CN corresponding to the higher values of $K_1 : CN \rightarrow EMCI$

(b) Connectome of EMCI corresponding to the higher values of $K_2 : EMCI \rightarrow LMCI$

(c) Connectome of LMCI corresponding to the higher values of $K_3 : LMCI \rightarrow AD$

(d) Connectome of CN corresponding to the higher values of $K_4 : CN \rightarrow AD$

Fig. 8. Brain connectivity network showing all the connections filtered by the action of K (filter: 0.01) during the progression from CN to EMCI, EMCI to LMCI, LMCI to AD, and directly from CN to AD.

from CN → EMCI, with frontal connectivity destruction. Lateralization is more visible in the last connectome, and there is a dramatic decrease in connectivity in the temporal area for the LMCI patient.

Getting back to K as a filtering tool for the connectome representation, we obtain glass brains for the progression from CN → EMCI, EMCI →LMCI, LMCI →AD, and CN → AD (see Fig. 8).

The comparison of CN→EMCI with EMCI→LMCI confirms the trend of occipital connectivity decrease, temporal-cerebellar connectivity diminution, and prefrontal alteration as also found by [38]. The smooth transition from LMCI → AD does not show any great change in the occipital lobe, as the effect was already visible from CN → EMCI. **We can thus wonder if the occipital lobe is one of the first areas to be damaged**; however, the evidence presented in [8] does not seem to support this hypothesis. From LMCI → AD, the connectivity diminution in the fronto-parietal lobe and an increase in the cerebellum confirm the findings of [38], while the cerebellar-parietal connectivity diminution is stronger in our results than in theirs.

It is worth noting that, although we considered a single person for each stage, a similar comparison could be run by averaging different patients, grouped according to age and sex, and envisaging the common features of disease progression [38].

4. *K*-Operator prediction

The primary goal of this section is to investigate the potential application of the K-operator as a diagnostic tool in predicting the progression of Alzheimer-Perusini's disease using rs-fMRI data collected during the initial visit. In this study, we leverage the application of machine learning methodologies, specifically multi-layer perceptron, to forecast the K-operator to determine the progression of the disease based on the patients' connectivity matrix at the initial assessment. We predict the K-operator by the trained Multi-Layer Perceptron (MLP) for a test patient, i.e., patient C (Fig. 9(a)).

To assess the accuracy of $K_{predicted}$, a visual comparison with $K_{measured}$ for patient C (Fig. 9(b)) is performed. As it can be noticed by the comparison between the predicted and measured K-operator (Fig. 9), the correspondence is more related to cluster sparsity of (absolute values) entries than to the precise numeric values. Moreover, in Table 2, we propose a comparison between the most relevant clusters of ROI-ROI pairs for the predicted and measured K. Excluding some connectivity alterations that are visible in the measured K but not in the predicted one, such as between putamen and thalamus pulvinar, we see that the main clusters obtained in $K_{measured}$ have also been identified in $K_{predicted}$, namely thalamus pulvinar, frontal superior medial, occipital,
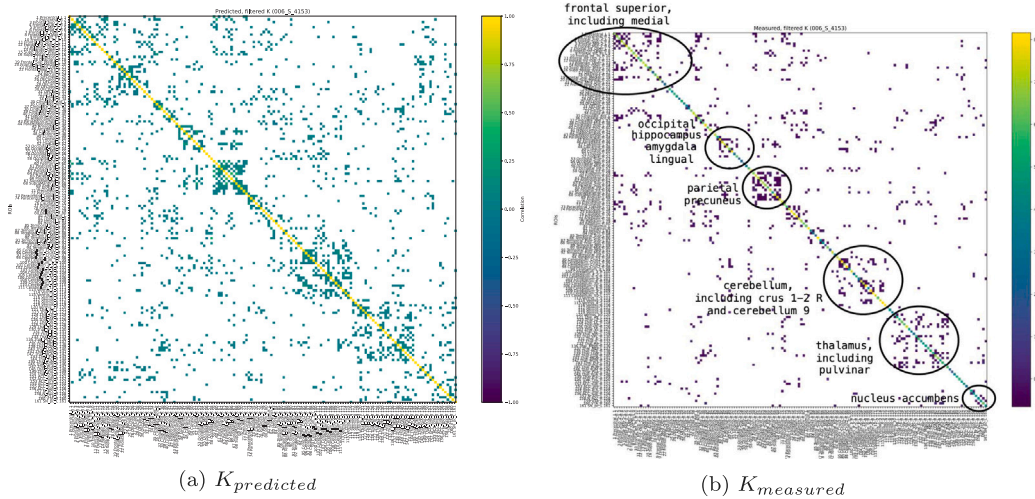
(a) $K_{predicted}$ (b) $K_{measured}$

Fig. 9. Predicted (MLP) and measured K-operator between the baseline and the first follow-up for a test male AD patient (patient C). Thresholds equal to 0.03 and 0.15, respectively.

Table 2
Correspondence of connectivity alteration between predicted and measured K, respectively, from Fig. 9. ACC stands for anterior cingulate cortex; x indicates disagreement between K predicted and measured.

	Frontal Sup. Med.	Occipital	Parietal	Amygdala	Angular	Cerebellum Crus 1-2R	Cereb. 9	Putamen	Thalamus Pulv.	Nucleus Acc.	ACC
Frontal Sup. Med.	✓										
Occipital		✓				✓					
Parietal			✓								
Amygdala				✓							
Angular					✓						
Cereb. Crus 1-2R		✓				✓	✓				
Cereb. 9						✓	✓				
Putamen									✓		
Thalamus Pulv.								x	✓	x	
Nucleus Acc.									x	✓	
ACC									✓		

cerebellum crus 1 and 2R, cerebellum IX, amygdala, nucleus accumbens, thus providing encouraging indications about the use of the K-operator prediction to determine the progression of the disease.

Then, let us focus on the connectome of patient C; using the K-operator as a predictor starting from the baseline, we obtain a predicted follow-up for patient C to be compared with the measured follow-up (see Fig. 10).

The connectomes measured respectively at the baseline and follow-up for patient C, where the links corresponding to the areas more affected by $K_{measured}$, are presented in Figs. 11(a) and 11(b), respectively.

We evaluate the prediction of the K-operator by adopting two different techniques represented by Eqs. (4) and (5) in Section 2.1. We first predict the connectome at the follow-up for patient C, where the intensity of the link strength is predicted according to the element-wise K strategy (Fig. 11(c)). On the contrary, the prediction of the follow-up for patient C, where the intensity of the link strength is predicted according to the row-by-column K strategy, and the choice of which links has to be modified is based on element-wise K, leads to a result (Fig. 11(d)), to be compared with the effective follow-up (Fig. 11(b)).

Thus, focusing on the connectomes of patient C, from the baseline (see Fig. 11(a)) to the measured follow-up (see Fig. 11(b)), an increase
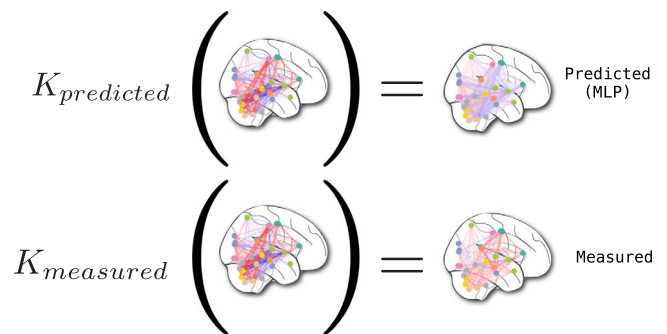
Fig. 10. Brain network from the baseline to the first follow-up, both predicted (up, right) and measured (down, right) for a test patient (i.e., patient C). The scale for the predicted connectome is smaller.

of cerebellar connectivity and a decrease of occipital connectivity are found. In these figures, for the sake of graphical clarity, we are only showing the links corresponding to the higher values of K (with sign).

Looking at Fig. 11(c), a decreased connectivity involving vermis

(a) Measured baseline, patient C. Links corresponding to all the areas more affected by K (threshold 0.05). Using $K_{measured}$ for the number of links.

(b) Measured follow-up, patient C. Links corresponding to all the areas more affected by K (threshold 0.05). Using $K_{measured}$ for the number of links.
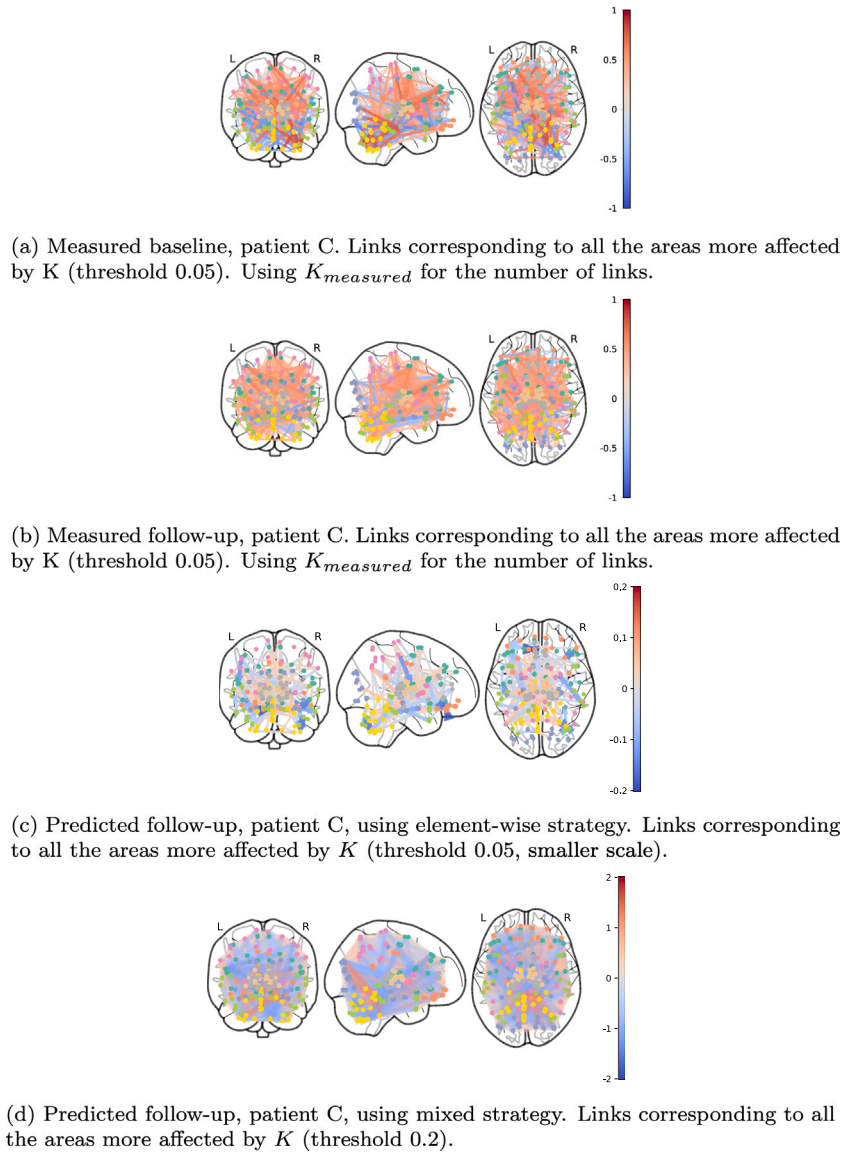

(c) Predicted follow-up, patient C, using element-wise strategy. Links corresponding to all the areas more affected by K (threshold 0.05, smaller scale).

(d) Predicted follow-up, patient C, using mixed strategy. Links corresponding to all the areas more affected by K (threshold 0.2).

Fig. 11. Comparison between measured and predicted connectomes of patient C.

and occipital lobe are correctly identified as in the measured follow-up (Fig. 11(b)). In addition, we have an effect of fronto-parietal connectivity diminution, inter-hemispheric, and frontal-cerebellar connectivity diminution. The element-wise K-strategy allows us to identify a a decline in local connectivity within the cerebellum.

Conversely, the connectomes obtained by adopting the mixed technique shown in Fig. 11(d) yield a result closer to the actual evolution, concerning an overall diminution of connectivity (Fig. 11(b)). The most important information is the decrease of frontal-cerebellum connectivity, not too visible in the actual follow-up of patient C, but relevant for the disease's evolution. This observation is based on the visual comparison of the red links between parietal and cerebellum in Fig. 11(d), in contrast with the prevailing gray or lines, indicating low or negative connectivity in Fig. 11(c).

Hence, the mixed approach, where links are selected according to the element-wise K while the "content" of the prediction is based on the classic product, provides a predicted follow-up brain network

reproducing some features closer to the effective one, rather than the K-prediction techniques based on the single element-wise strategy. These results show how the element-wise product can be used to find the brain areas most impacted by the disease and the classic product for the actual values of the change.

5. Discussions

Alzheimer-Perusini's disease (AD) represents a complex group of neurodegenerative disorders characterized by a range of symptoms, including short-term memory impairment and decline in bodily functions, ultimately leading to mortality [44]. The progressive nature of AD significantly reduces the overall life satisfaction and well-being of the elderly affected by the condition. Despite significant investment over several decades, an effective treatment for AD has not yet been developed. Most clinical trials in AD research have yielded unsuccessful

results in developing efficacious treatments [45–47]. The elevated incidence of treatment failure may be attributed to the timing of treatment administration, as it may be delayed until the onset of symptomatic dementia [45]. Moreover, the significant underdiagnosis of AD is particularly noteworthy, especially within the primary care context [48]. In a study involving older adults with suspected dementia, 58.7% were found to either not have received a formal diagnosis (39.5%) or were unaware (19.2%) of their condition [49]. There is a growing body of evidence indicating that early identification of Alzheimer-Perusini's disease is essential. This early recognition not only allows patients with AD to implement timely preventive measures (such as diet and lifestyle changes) but also assists researchers in better identifying and characterizing clinical trial participants. The neurodegenerative mechanisms implicated in AD disease start years before the onset of clinical symptoms and formal diagnoses, thereby offering a substantial timeframe for the early prediction and detection of potential risk factors associated with the condition [50].

This study investigated the potential application of a mathematical operator as a diagnostic tool for predicting the progression of AD based on rs-fMRI data obtained at an initial visit. The results of our investigation demonstrate that predictive modeling yields outcomes that align more closely with the eventual progression of Alzheimer-Perusini's disease. Therefore, with an understanding of the specific brain regions susceptible to change, targeted interventions can be implemented to minimize further deterioration.

The proposed approach is based on extracting information from functional magnetic resonances at the resting state; thus, it is important to consider which areas receive an increased blood flow during the resting state to compare healthy and pathological states. The more involved areas at the resting state constitute the so-called *default mode network*. According to [43], in healthy individuals, the clusters constituting the subcortical default mode network correspond to **anterior cingulate cortex**, **precuneus**, inferior **parietal** lobule, **angular gyrus**, **medial frontal pole**, ventromedial **prefrontal cortex**, anterior and middle **parahippocampal gyrus**, ventral tegmental area, caudate nucleus, nucleus accumbens. They strictly interact with **hippocampus**, cerebellum, **thalamus**, **amygdala**, right **crus I/II** and lobule and cerebellar **vermis IX** [43].

This is the rationale behind our comments on the K-operator assessment, which is primarily centered on examining specific brain regions, including the nucleus accumbens, amygdala, lingual gyrus, precuneus, ventral tegmental area, occipital cortex, and hippocampus. Mainly, we found that the progression of AD patients presents an alteration of connectivity between the amygdala and parahippocampal gyrus, frontal superior area, between ventral tegmental area and anterior cingulate cortex. Moreover, damage to connectivity between some cerebellar areas and the temporal lobe is also detected.

Moreover, as known from [8], Alzheimer-Perusini's disease starts with the medial temporal lobe (preclinical AD, asymptomatic), then spreads to lateral temporal and parietal lobes (MCI due to AD), subsequently reaching the frontal lobe, and finally involves the occipital lobe. However, according to [38], damage to the occipital lobe is also occurring at the stage of EMCI and LMCI, and not only for severe AD cases. Authors in [38] identify the brain areas more impacted by AD as the frontal anterior cortex, default mode network, frontoparietal, and somatomotor areas. The default mode network is relevant for emotional processing and memory, the frontoparietal lobe for cognition, and the somatomotor for skill learning and sensory perception. The authors of the same study also found a shift toward the random network organization and a more integrated local structure, also considering the transition from CN to EMCI, to LMCI, to AD. Our results mostly confirm these findings. We also confirm the findings of [43] concerning the subcortical default mode network as detailed in Section 3, and also noticed a clear effect of nucleus accumbens and ventral tegmental area, not found by [43] for possible resolution problems (as stated by the author themselves), but visible in our K-operators, and supported by our previous study [15].

6. Conclusions

Memory impairment is a prominent manifestation experienced by individuals afflicted by specific neurological disorders such as Alzheimer-Perusini's disease. In our research, we propose a method to extract information from AD data and predict the disease's progression, through a matrix operator derived from the connectivity matrices. The current study employs a physics-inspired mathematical operator, designated as K, that has recently been proposed to conceptualize a broad neurological disorder based on resting-state functional magnetic resonance imaging (rs-fMRI) data. Building upon initial empirical observations, we are presently implementing this operator in analyzing the real-world data obtained from the Alzheimer's Disease Neuroimaging Initiative (ADNI). Our application's findings align with those reported in the medical literature, particularly with regard to the involvement of the default network mode, posterior cingulate, and hypothalamus in their dysregulation in AD, in addition to the disease's impact on the temporal lobe and subcortical structures.

Additionally, the study explores the potential utility of the K-operator as a diagnostic instrument for forecasting AD advancement through analysis of rs-fMRI data. The study's findings revealed that the thalamus pulvinar, frontal superior medial, anterior cingulate cortex, angular, precuneus, occipital, fusiform, cerebellum crus 1 and 2R, and cerebellum IX demonstrated significant alterations, as detected by our prediction model. The concurrence of these clusters with those identified by direct measurement offers promising support for the utility of the K-operator in predicting disease progression.

Limitations. The restricted sample of patients is the main limitation of our research. In fact, the proposed approach employed only a limited number of patients' rs-fMRI images that encompass all the requisite features for our analysis and forecasting. We are currently conducting an in-depth analysis of resting-state functional magnetic resonance imaging data from AD patients to extend our findings to a larger and more diverse sample of participants. Including a higher number of subjects might also help quantify the degree of inter-person variability, both for healthy and for diseased patients.

Future directions. Future research can refine the prediction of disease progression, fostering an additional tool to help physicians tune the personalized therapy and intervention for the patients. A matrix-based method, inspired by physics, can also help deepen the understanding of a disease compared to a related one, as the contraposition between AD, mainly a defect of memory, and its opposite, the hyperthymesia. The last one was defined in 2006 as Highly-Superior Autobiographical Memory (HSAM) but already described in the novel Funes by J. G. Borges. Conceptually, hyperthymesia is somehow the inverse disease of Alzheimer-Perusini's one. A future differential investigation can consider the clusters obtained for both diseases, expecting that the K-operator will have opposite features.

Analyzing the fMRI of a single hyperthymetic patient, [51] find a variation of connectivity mostly involving the lingual gyrus, precuneus, fusiform gyrus, cerebellum, middle and superior frontal gyrus, the areas also involved in the "opposite" disease, i.e., AD. The anatomic analysis of brains of hyperthymetic (or HSAM) patients shows effects on subcortical nuclei, mediotemporal-limbic, and temporo-occipital regions [52], while a resting-state fMRI comparison between HSAM patients and healthy controls highlight alterations involving mediotemporal, limbic, prefrontal pathways, also related to language and memory [52]. Considering the so-called "normality" in terms of statistical balance between these two effects of memory alteration, a differential analysis of these diseases, helped by the respective K-operators and their inverse operators, the healing H, we can imagine the development of new therapies and new drugs.
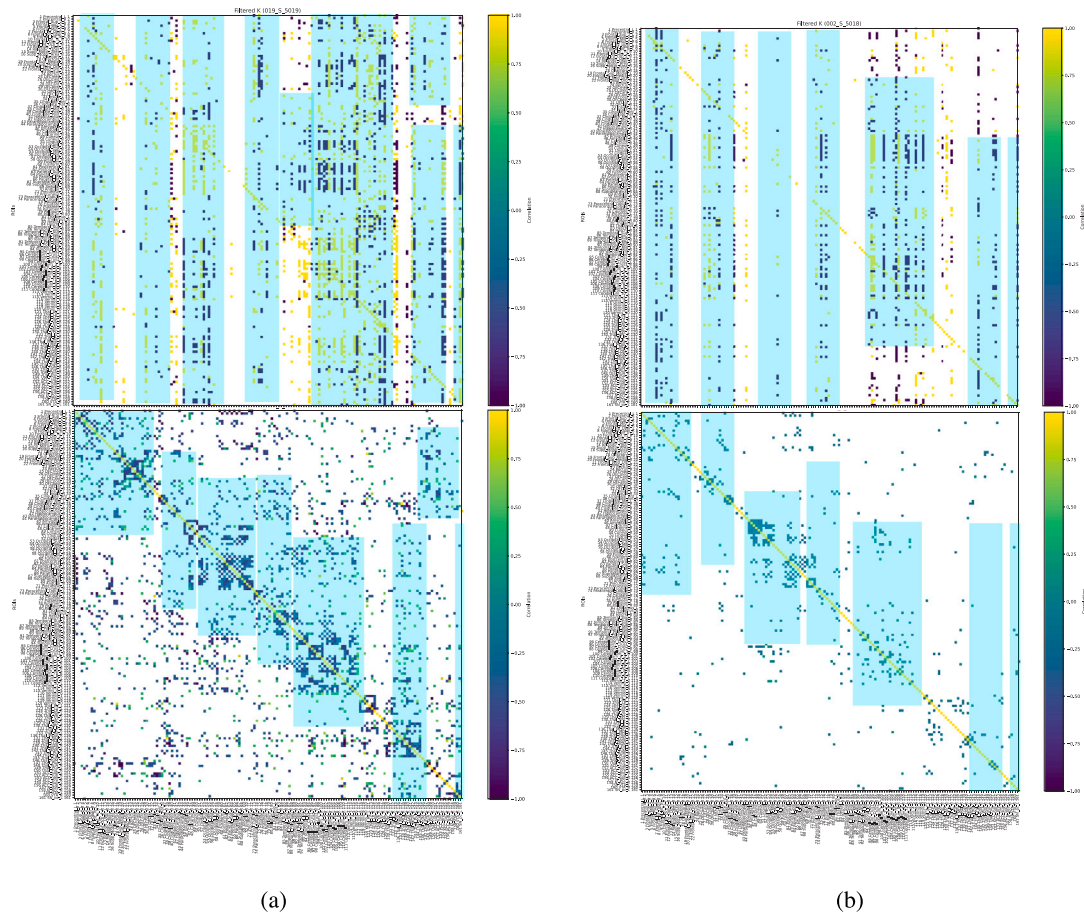
Fig. 12. Block correspondence of the *K*-operators computed with the classic (top) and the hybrid product (down), for patients A (a) and B (b). To magnify the two images, click here and here, respectively.

CRediT authorship contribution statement

Maria Mannone: Writing – review & editing, Writing – original draft, Visualization, Validation, Software, Methodology, Investigation, Formal analysis, Data curation, Conceptualization. **Norbert Marwan:** Writing – review & editing, Supervision, Methodology, Conceptualization. **Peppino Fazio:** Writing – review & editing, Supervision, Conceptualization. **Patrizia Ribino:** Writing – review & editing, Writing – original draft, Validation, Supervision, Project administration, Methodology, Investigation, Funding acquisition, Formal analysis, Data curation, Conceptualization.

Declaration of competing interest

The authors declare that they have no known competing financial interests or personal relationships that could have appeared to influence the work reported in this paper.

Acknowledgments

Code availability

The codes can be accessed at: https://github.com/medusamedusa/AAL3_K-operator_AD.

Appendix

Table with the ROI

See Table A.3.

Comparison between products

See Fig. 12.

Data availability

Data used for preparation of this article were obtained from the Alzheimer's Disease Neuroimaging Initiative (ADNI) database (https://adni.loni.usc.edu). As such, the investigators within the ADNI contributed to the design and implementation of ADNI and/or provided data but did not participate in the analysis or writing of this report. A complete listing of ADNI investigators can be found at: https://adni.loni.usc.edu/wp-content/uploads/how_to_apply/ADNI_Acknowledgement_

Table A.3

The considered ROIs from the AAL3 atlas. SN_pc_L (substantia nigra pars reticulata, left) does not appear in the prediction and in the progression CN→AD, for reduced readability of some of the images.

ROI label	Brain lobe
Precentral_L 1	Frontal
Precentral_R 2	Frontal
Frontal_Sup_2_L 3	Frontal
Frontal_Sup_2_R 4	Frontal
Frontal_Mid_2_L 5	Frontal
Frontal_Mid_2_R 6	Frontal
Frontal_Inf_Oper_L 7	Frontal
Frontal_Inf_Oper_R 8	Frontal
Frontal_Inf_Tri_L 9	Frontal
Frontal_Inf_Tri_R 10	Frontal
Frontal_Inf_Orb_2_L 11	Orbitofrontal
Frontal_Inf_Orb_2_R 12	Orbitofrontal
Rolandic_Oper_L 13	Frontal
Rolandic_Oper_R 14	Frontal
Supp_Motor_Area_L 15	Frontal
Supp_Motor_Area_R 16	Frontal
Olfactory_L 17	Frontal
Olfactory_R 18	Frontal
Frontal_Sup_Medial_L 19	Frontal
Frontal_Sup_Medial_R 2	Frontal
Frontal_Med_Orb_L 21	Orbitofrontal
Frontal_Med_Orb_R 22	Orbitofrontal
Rectus_L 23	Frontal
Rectus_R 24	Frontal
OFCmed_L 25	Orbitofrontal
OFCmed_R 26	Orbitofrontal
OFCant_L 27	Orbitofrontal
OFCant_R 28	Orbitofrontal
OFCpost_L 29	Orbitofrontal
OFCpost_R 30	Orbitofrontal
OFClat_L 31	Orbitofrontal
OFClat_R 32	Orbitofrontal
Insula_L 33	Insula
Insula_R 34	Insula
Cingulate_Ant_L 35	Limbic
Cingulate_Ant_R 36	Limbic
Cingulate_Mid_L 37	Limbic
Cingulate_Mid_R 38	Limbic
Cingulate_Post_L 39	Limbic
Cingulate_Post_R 40	Limbic
Hippocampus_L 41	Limbic
Hippocampus_R 42	Limbic
ParaHippocampal_L 43	Limbic
ParaHippocampal_R 44	Limbic
Amygdala_L 45	Limbic
Amygdala_R 46	Limbic
Calcarine_L 47	Occipital
Calcarine_R 48	Occipital
Cuneus_L 49	Occipital
Cuneus_R 50	Occipital
Lingual_L 51	Occipital
Lingual_R 52	Occipital
Occipital_Sup_L 53	Occipital
Occipital_Sup_R 54	Occipital
Occipital_Mid_L 55	Occipital
Occipital_Mid_R 56	Occipital
Occipital_Inf_L 57	Occipital
Occipital_Inf_R 58	Occipital
Fusiform_L 59	Temporal
Fusiform_R 60	Temporal

Table A.3 (*continued*).

ROI label	Brain lobe
Postcentral_L 61	Parietal
Postcentral_R 62	Parietal
Parietal_Sup_L 63	Parietal
Parietal_Sup_R 64	Parietal
Parietal_Inf_L 65	Parietal
Parietal_Inf_R 66	Parietal
SupraMarginal_L 67	Parietal
SupraMarginal_R 68	Parietal
Angular_L 69	Parietal
Angular_R 70	Parietal
Precuneus_L 71	Parietal
Precuneus_R 72	Parietal
Paracentral_Lobule_L 73	Parietal
Paracentral_Lobule_R 74	Parietal
Caudate_L 75	Subcortical
Caudate_R 76	Subcortical
Putamen_L 77	Subcortical
Putamen_R 78	Subcortical
Pallidum_L 79	Subcortical
Pallidum_R 80	Subcortical
Thalamus_L 81	Subcortical
Thalamus_R 82	Subcortical
Heschl_L 83	Temporal
Heschl_R 84	Temporal
Temporal_Sup_L 85	Temporal
Temporal_Sup_R 86	Temporal
Temporal_Pole_Sup_L 87	Temporal
Temporal_Pole_Sup_R 88	Temporal
Temporal_Mid_L 89	Temporal
Temporal_Mid_R 90	Temporal
Temporal_Pole_Mid_L 91	Temporal
Temporal_Pole_Mid_R 92	Temporal
Temporal_Inf_L 93	Temporal
Temporal_Inf_R 94	Temporal
Cerebellum_Crus1_L 95	Cerebellum
Cerebellum_Crus1_R 96	Cerebellum
Cerebellum_Crus2_L 97	Cerebellum
Cerebellum_Crus2_R 98	Cerebellum
Cerebellum_3_L 99	Cerebellum
Cerebellum_3_R 100	Cerebellum
Cerebellum_4_5_L 101	Cerebellum
Cerebellum_4_5_R 102	Cerebellum
Cerebellum_6_L 103	Cerebellum
Cerebellum_6_R 104	Cerebellum
Cerebellum_7b_L 105	Cerebellum
Cerebellum_7b_R 106	Cerebellum
Cerebellum_8_R 108	Cerebellum
Cerebellum_9_L 109	Cerebellum
Cerebellum_9_R 110	Cerebellum
Cerebellum_10_L 111	Cerebellum
Vermis_1_2 113	Cerebellum
Vermis_3 114	Cerebellum
Vermis_4_5 115	Cerebellum
Vermis_6 116	Cerebellum
Vermis_7 117	Cerebellum
Vermis_8 118	Cerebellum
Vermis_9 119	Cerebellum
Vermis_10 120	Cerebellum
Thal_AV_L 121	Subcortical
Thal_AV_R 122	Subcortical
Thal_LP_L 123	Subcortical
Thal_LP_R 124	Subcortical
Thal_VA_L 125	Subcortical
Thal_VA_R 126	Subcortical
Thal_VL_L 127	Subcortical
Thal_VL_R 128	Subcortical
Thal_VPL_L 129	Subcortical
Thal_VPL_R 130	Subcortical
Thal_IL_L 131	Subcortical
Thal_IL_R 132	Subcortical
Thal_Re_L 133	Subcortical

Table A.3 (*continued*).

ROI label	Brain lobe
Thal_MDm_R 136	Subcortical
Thal_MDl_L 137	Subcortical
Thal_MDl_R 138	Subcortical
Thal_LGN_L 139	Subcortical
Thal_LGN_R 140	Subcortical
Thal_MGN_L 141	Subcortical
Thal_MGN_R 142	Subcortical
Thal_PuI_L 143	Subcortical
Thal_PuI_R 144	Subcortical
Thal_PuM_L 145	Subcortical
Thal_PuM_R 146	Subcortical
Thal_PuA_L 147	Subcortical
Thal_PuA_R 148	Subcortical
Thal_PuL_L 149	Subcortical
Thal_PuL_R 150	Subcortical
ACC_sub_L 151	Limbic
ACC_sub_R 152	Limbic
ACC_pre_L 153	Limbic
ACC_pre_R 154	Limbic
ACC_sup_L 155	Limbic
ACC_sup_R 156	Limbic
N_Acc_L 157	Subcortical
N_Acc_R 158	Subcortical
VTA_L 159	Subcortical
VTA_R 160	Subcortical
SN_pc_L 161	Subcortical

List.pdf. For patient C, given the incompleteness of the first DICOM folder, we used the second folder of 2011-11-04 (I264987), and the second folder of 2012-3-27 (I293809).

References

[1] J.L. Borges, Funes the memorious, 1942, https://vigeland.caltech.edu/ist4/lectures/funes%20borges.pdf.

[2] R. Quiroga, In retrospect: Funes the memorious, Nature 463 (611) (2010) http://dx.doi.org/10.1038/463611a.

[3] A.A. Brandon, E.P. Hussey, M.J. Donahue, A case of hyperthymesia: Rethinking the role of theamygdala in autobiographical memory, Neurocase 19 (2) (2013) 166–181, http://dx.doi.org/10.1080/13554794.2011.654225A.

[4] B. Ally, E.P. Hussey, M.J. Donahue, A case of hyperthymesia: rethinking the role of the amygdala in autobiographical memory, Neurocase 19 (2) (2013).

[5] B. Lucci, The contribution of gaetano perusini to the definition of Alzheimer's disease, Ital. J. Neurol. Sci. (1998) 49–52.

[6] P.M. Thompson, J. Moussai, S. Zohoori, A. Goldkorn, A.A. Khan, M.S. Mega, G.W. Small, J.L. Cummings, A.W. Toga, Cortical variability and asymmetry in normal aging and Alzheimer's disease, Cerebral Cortex 8 (6) (1998) 492–509, http://dx.doi.org/10.1093/cercor/8.6.492.

[7] M. McDonough, S.B. Festini, M.M. Wood, Risk for Alzheimer's disease: A review of long-term episodic memory encoding and retrieval fMRI studies, Age. Res. Rev. 62 (2020) 101133.

[8] S. Dan, D. Sharma, K. Rastogi, et al., Therapeutic and diagnostic applications of nanocomposites in the treatment Alzheimer's disease studies, Biointerf. Res. Appl. Chem. 12 (1) (2021) 940–960, http://dx.doi.org/10.33263/BRIAC121.940960.

[9] L.R. Squire, The legacy of patient HM for neuroscience, Neuron 61 (1) (2009) 6–9.

[10] L. Al-Ani, A. Tao, J. Dyke, G. Chiang, M. Ishii, Amygdala atrophy as an early manifestation of Alzheimer's disease, Neurology 100 (17) (2023) http://dx.doi.org/10.1212/WNL.0000000000202128.

[11] M.A. Rubin, J.E. Safdieh, Netter's Concise Neuroanatomy (Netter Basic Science), Saunders, 2007.

[12] M. Mannone, P. Fazio, N. Marwan, Modeling a neurological disorder as the result of an operator acting on the brain: A first sketch based on network channel modeling, Chaos (2024).

[13] M. Mannone, P. Fazio, J. Kurths, P. Ribino, N. Marwan, A brain-network operator for modeling disease: a first data-based application for Parkinson's disease, Eur. J. Phys. Spec. Top. (2024) URL https://link.springer.com/article/10.1140/epjs/s11734-024-01345-6.

[14] M. Mannone, P. Fazio, P. Ribino, N. Marwan, On disease and healing: A theoretical sketch, Front. Appl. Math. Stat. (19) (2024) http://dx.doi.org/10.3389/fams.2024.1468556.

[15] M. Mannone, P. Fazio, N. Marwan, P. Ribino, K-operator as a predictor for Alzheimer-Perusini's disease, in: Proceedings of the HCist – International Conference on Health and Social Care Information Systems and Technologies, 2024, 2024, http://dx.doi.org/10.5281/zenodo.13150406, in press.

[16] E.T. Rolls, C.C. Huang, C.-P. Lin, J. Feng, M. Joliot, Automated anatomical labelling atlas 3, Neuroimage 206 (2020) 116189, http://dx.doi.org/10.1016/j.neuroimage.2019.116189.

[17] M. Clos, N. Bunzeck, T. Sommer, Dopamine is a double-edged sword: Dopaminergic modulation enhances memory retrieval performance but impairs metacognition, Neuropsychopharmacology 44 (3) (2019) 555–563, http://dx.doi.org/10.1038/s41386-018-0246-y.

[18] A. Pathak, D. Roy, A. Banerjee, Whole-brain network models: From physics to bedside, Front. Comput. Neurosci. 16 (866517) (2022) http://dx.doi.org/10.3389/fncom.2022.866517.

[19] P. beim Graben, J. Kurths, T. Liebscher, Neural and cognitive modeling with networks of leaky integrator units, in: P. beim Graben, C. Zhou, M. Thiel, J. Kurths (Eds.), Understanding Complex Systems, in: Lectures in Supercomputational Neuroscience: Dynamics in Complex Brain Networks, Springer, Berlin, 2008, http://dx.doi.org/10.1007/978-3-540-73159-7_7.

[20] R. Tripathi, B.J. Gluckman, Development of mechanistic neural mass (mNM) models that link physiology to mean-field dynamics, Front. Netw. Physiol. 2 (2022) 911090.

[21] W.W. Seeley, Mapping Neurodegenerative Disease Onset and Progression, Cold Spring Harb Perspect. Biol. 9 (a023622) (2017) 1–18, URL https://cshperspectives.cshlp.org/content/9/8/a023622.full.pdf.

[22] J. Royer, B.C. Bernhardt, S. Larivière, E. Gleichgerrcht, B.J. Vorderwülbecke, S. Vulliémoz, L. Bonilha, Epilepsy and brain networks hubs, Epilepsia 63 (2022) 537–550.

[23] F. Bartolomei, M. Guye, F. Wendling, Abnormal binding and disruption in large scale networks involved in human partial seizures, EPJ Nonlinear Biomed. Phys. 1 (4) (2013) 1—16.

[24] M.P. van den Heuvel, R.C. Mandl, C.J. Stam, R.S. Kahn, H.E.H. Pol, Aberrant frontal and temporal complex network structure in schizophrenia: A graph theoretical analysis, J. Neurosci. 30 (47) (2010) 15915–15926.

[25] John C. Morris, The Clinical Dementia Rating (CDR) current version and scoring rules, Neurology 43 (11) (1993) 2412.

[26] Janine Bijsterbosch, Stephen M. Smith, Christian Beckmann, An Introduction to Resting State fMRI Functional Connectivity, Oxford University Press, 2017.

[27] Oleg S. Pianykh, Digital Imaging and Communications in Medicine (DICOM): A Practical Introduction and Survival Guide, vol. 10, Springer, 2012.

[28] G. Varoquaux, A. Gramfort, F. Pedregosa, V. Michel, B. Thirion, Multisubject dictionary learning to segment an atlas of brain spontaneous activity, Inf. Process. Med. Imag. (2011) 562–573.

[29] D. Kennedy, C. Haselgrove, J. Breeze, J. Frazier, L. Seidman, J. Goldstein, HarvardOxford cort maxprob thr25 2mm URL https://fsl.fmrib.ox.ac.uk/fsl/fslwiki/Atlases.

[30] N. Tzourio-Mazoyer, B. Landeau, D. Papathanassiou, F. Crivello, O. Étard, N. Delcroix, B. Mazoyer, M. Joliot, Automated anatomical labeling of activations in SPM using a macroscopic anatomical parcellation of the MNI mri single-subject brain, Neuroimage 15 (2002) 273–289, http://dx.doi.org/10.1006/nimg.2001.0978.

[31] E.T. Rolls, M. Joliot, N. Tzourio-Mazoyer, Implementation of a new parcellation of the orbitofrontal cortex in the automated anatomical labeling atlas, Neuroimage 122 (2015) 1–5, http://dx.doi.org/10.1016/j.neuroimage.2015.07.075.

[32] P. Krashia, E. Spoleti, M. D'Amelio, The VTA dopaminergic system as diagnostic and therapeutical target for Alzheimer's disease, Front. Psychiatry 13 (1039725) (2022).

[33] H.-A. Yi, et al., Relation between subcortical grey matter atrophy and conversion from mild cognitive impairment to Alzheimer's disease, J. Neurol. Neurpsurg. Psychiatry 87 (4) (2015).

[34] Y. Chen, T. Chen, R. Hou, Locus coeruleus in the pathogenesis of Alzheimer's disease: A systematic review, Transl. Res. Clin. Interv. 8 (1) (2022) e12257, http://dx.doi.org/10.1002/trc2.12257.

[35] R.P. Vertes, S.B. Linley, W.B. Hoover, Limbic circuitry of the midline thalamus, Neurosci. Biobehav. Rev. 54 (2015) 89–107, http://dx.doi.org/10.1016/j.neubiorev.2015.01.014.

[36] F.L. Stevens, R.A. Hurley, K.H. Taber, Distinct alterations in cerebellar connectivity with substantia nigra and ventral tegmental area in Parkinson's disease, Windows Brain 23 (2) (2011).

[37] I.M. O'Shea, H.S. Popal, I.R. Olson, et al., Distinct alterations in cerebellar connectivity with substantia nigra and ventral tegmental area in Parkinson's disease, Sci. Rep. 12 (3289) (2022) http://dx.doi.org/10.1038/s41598-022-07020-x.

[38] A. Fathian, Y. Jamali, M.R. Raoufy, et al., The trend of disruption in the functional brain network topology of Alzheimer's disease, Sci. Rep. 12 (14998) (2022) http://dx.doi.org/10.1038/s41598-022-18987-y.

[39] P. Eustache, et al., Multimodal magnetic resonance imaging in Alzheimer's disease patients at prodromal stage, J. Alzheimer's Dis. 50 (4) (2016) 1035–1050, http://dx.doi.org/10.3233/JAD-150353.

[40] K.M. Stouffer, X. Grande, E. Düzel, M. Johansson, B. Creese, M.P. Witter, M.I. Miller, L.E.M. Wisse, D. Berron, Amidst an amygdala renaissance in Alzheimer's disease, Brain 147 (2024) 816–829.

[41] Stephanie Rudolph, Aleksandra Badura, Stefano Lutzu, Salil Saurav Pathak, Andreas Thieme, Jessica L. Verpeut, Mark J. Wagner, Yi-Mei Yang, Diasynou Fioravante, Cognitive-affective functions of the cerebellum, J. Neurosci. 43 (45) (2023) 7554–7564.

[42] Jeremy D. Schmahmann, The cerebellum and cognition, Neurosci. Lett. 688 (2019) 62–75.

[43] S. Seoane, M. van den Heuvel, A. Acebes, N. Janssen, The subcortical default mode network and Alzheimer's disease: a systematic review and meta-analysis, Brain Commun. (2024) URL https://www.medrxiv.org/content/10.1101/2023.10.02.23296420v1.full.pdf.

[44] Mark P. Mattson, Pathways towards and away from Alzheimer's disease, Nature 430 (7000) (2004) 631–639.

[45] Dev Mehta, Robert Jackson, Gaurav Paul, Jiong Shi, Marwan Sabbagh, Why do trials for Alzheimer's disease drugs keep failing? A discontinued drug perspective for 2010–2015, Expert Opin. Investig. Drugs 26 (6) (2017) 735–739.

[46] Camryn Berk, Gaurav Paul, Marwan Sabbagh, Investigational drugs in Alzheimer's disease: Current progress, Expert Opin. Investig. Drugs 23 (6) (2014) 837–846.

[47] Anita Slomski, Another amyloid-beta blocker fails to halt dementia, JAMA 321 (24) (2019) 2396.

[48] Joseph Gaugler, Bryan James, Tricia Johnson, Jessica Reimer, Michele Solis, Jennifer Weuve, Rachel F. Buckley, Timothy J. Hohman, 2022 Alzheimer's disease facts and figures, Alzheimers Dementia 18 (4) (2022) 700–789.

[49] Halima Amjad, David L. Roth, Orla C. Sheehan, Constantine G. Lyketsos, Jennifer L. Wolff, Quincy M. Samus, Underdiagnosis of dementia: an observational study of patterns in diagnosis and awareness in US older adults, J. Gen. Intern. Med. 33 (2018) 1131–1138.

[50] Marta Crous-Bou, Carolina Minguillón, Nina Gramunt, José Luis Molinuevo, Alzheimer's disease prevention: from risk factors to early intervention, Alzheimer's research & therapy 9 (2017) 1–9.

[51] G. Mazzoni, A. Clark, A. De Bartolo, C. Guerrini, Z. Nahouli, D. Duzzi, M. De Marco, W. McGeown, A. Venneri, Brain activation in highly superior autobiographical memory: The role of the precuneus in the autobiographical memory retrieval network, Cortex 120 (2019) 588–602.

[52] J. Talbot, G. Convertino, M. De Marco, A. Venneri, G. Mazzoni, Highly superior autobiographical memory (HSAM): A systematic review, Neuropsychol. Rev. (2024).